

## Monte Carlo Trajectory Calculations of Atomic Excitation and Ionization by Thermal Electrons\*

Peter Mansbach<sup>†</sup> and James Keck<sup>‡</sup>

*Avco Everett Research Laboratory, Everett, Massachusetts*

(Received 23 December 1968)

The excitation and de-excitation of atoms by electron impact has been investigated for states near the ionization limit using classical Monte Carlo trajectory calculations. The trajectories were sampled within the reaction zone with a weight proportional to the equilibrium reaction rate and integrated backward and forward in time to obtain complete histories for the collisions. This method is very much more efficient than the usual technique of sampling outside the reaction zone, and makes an otherwise extremely expensive calculation feasible. The results indicate that for energy transfers less than a few  $kT$  the reaction cross-section is determined by adiabatic collisions, while for transfers greater than a few  $kT$  the impulse approximation is valid. The data have been used to obtain the following convenient approximation for the equilibrium transition kernel valid near the ionization limit:

$$R(E_f, E_i) = 7.8 \times 10^{-26} [A^+]_e [e]_e^2 [kT(\text{eV})]^{-13/2} (-E_</math>$$

where  $E_< = \min(E_i, E_f)$ , and  $E_> = \max(E_i, E_f)$ . This has been used in conjunction with a conventional master equation to obtain an exact expression for the steady state collisional recombination rate constant  $a = 2.0 \times 10^{-27} [e] [kT(\text{eV})]^{-9/2} \text{cm}^3/\text{sec}$ . Comparison with the available experimental data is reasonably good, but there are indications that both radiative cascading and collisions with neutrals may be important under some experimental conditions.

### I. INTRODUCTION

It has been shown by Keck<sup>1</sup> that Monte Carlo trajectory calculations can be efficiently used in conjunction with the variational theory of reaction rates<sup>2</sup> to determine equilibrium transition probabilities for molecular systems by sampling within the reaction zone. Such transition probabilities may then be substituted into a conventional master equation<sup>3</sup> or corresponding diffusion equation<sup>4</sup> to study the behavior of nonequilibrium reactions.

In the present paper we treat the problem of excitation and ionization of hydrogenlike atoms by collision with thermal electrons. A major aim of the investigation is to determine the effect of adiabatic collisions on the energy transfer between states near the dissociation limit. This is important for assessing the validity of the impulse approximation and cutoff procedures used by Gryzinski<sup>5, 6</sup> in his classical theory of electronic excitation, and by Bates, Kingston, and McWhirter<sup>7</sup> in their numerical investigations of collisional-radiative recombination. It is also important for assessing the validity of the Fokker-Planck equation used by Gurevich and Pitaevskii<sup>8</sup> in their treatment of collisional cascading. As will be shown, none of the above approximation is really valid though they all give results of the right order of magnitude.

Similar studies have been carried out by Abrines, Percival, and Valentine<sup>9</sup> who used Monte Carlo methods in conjunction with the usual impact parameter formulation<sup>10</sup> to calculate cross sections

for direct ionization by monoenergetic electrons. Although this process is important for ionization by electron beams at low densities where collisional de-excitation is negligible compared to radiative de-excitation, it plays a minor role in thermal plasmas at normal densities where ionization proceeds primarily by collisional cascading. Thus the work of Abrine, Percival, and Valentine is largely complementary to the present work in which the emphasis was on cascading, and only a small fraction of the collisions studied resulted in direct ionization. Where the results do overlap, however, they are in general agreement, and the qualitative conclusions which may be drawn concerning the range of validity of classical mechanics and the impulse approximation are identical.

In Sec. II we derive the integrals and the statistical methods used to obtain our numerical data. Section III is a summary of our results and of convenient approximate expressions. These are compared with the results obtained by Gryzinski. In Sec. IV we use our expressions in conjunction with a master equation to obtain a recombination rate constant which is then compared with available experimental data.

### II. MATHEMATICAL MODEL

Following Gryzinski, we assume that a strictly classical treatment can be applied. This assumption is valid as long as we restrict our considerations to states near the dissociation limit where

the principal quantum number is large. Under this condition a system composed of a neutral atom consisting of one excited electron orbiting about a point core, and one free electron, can be represented by a point in an 18 dimensional phase space which behaves in accordance with classical laws under the influence of the Coulomb interactions. Our coordinates are chosen to be the position  $\vec{R}$  and momentum  $\vec{P}$  of the core (which we take to be the center-of-mass), the position  $\vec{r}_1$  and momentum  $\vec{p}_1$  of the bound electron with respect to the nucleus, and the position  $\vec{r}_2$  and momentum  $\vec{p}_2$  of the free electron with respect to the nucleus. The energy of the atom can then be written  $E_1 = (\vec{p}_1^2/2m) - e^2/r_1$ , where  $m$  is the electron mass.

We now define the equilibrium transition kernel  $R(E_f, E_i)$  to be the rate of transition from  $E_1 = E_i$  to  $E_1 = E_f$ , per unit volume, per unit initial and final energies, for a plasma in complete thermodynamic equilibrium. Note that  $R(E_f, E_i)$  is symmetric in its arguments; hence, we shall only consider the case  $E_f < E_i$ , i. e., de-excitation. Since we have assumed a classical system,  $E_1$  must take on all values between  $E_i$  and  $E_f$  in the course of a collision. Consequently, a rigorous upper bound to  $R(E_f, E_i)$  will be given by the rate  $\mathcal{R}_S$  at which atoms cross a surface in phase space defined by  $E_1 = E_S$ , in the downward (decreasing  $E_1$ ) direction, where  $E_i > E_S > E_f$  [see Fig. 1(a)]. This rate is given by the variational theory as<sup>2</sup>

$$\mathcal{R}_S = V^{-1} \int_S \rho_e \vec{v} \cdot \vec{n} dS, \quad (\text{II. 1})$$

where  $V$  is the normalization volume,  $\rho_e$  is the equilibrium density of points in phase space,  $\vec{v}$  is the generalized velocity of a point in phase space,  $\vec{n}$  is the unit normal to the surface element  $dS$  and the integration is over that part  $S$  of the surface  $E_1 = E_S$  on which  $\vec{v} \cdot \vec{n} < 0$ , i. e., atoms are being de-excited.

The rate  $\mathcal{R}_S$  is an overestimate of  $R(E_f, E_i)$  for two reasons. The first is that only a few of the atoms passing through  $E_S$  started at  $E_i$  and will end at  $E_f$ . The second is that even those atoms which do go from  $E_i$  to  $E_f$  may pass through  $E_S$  more than once, as shown in Fig. 1(b). This happens because the bound electron revolves around the nucleus and alternately gains and loses energy to the free electron. Thus, for  $E_i > E_S > E_f$  we can define a fraction  $f_S(E_f, E_i) \leq 1$  such that

$$R(E_f, E_i) = f_S(E_f, E_i) \mathcal{R}_S. \quad (\text{II. 2})$$

To determine  $f_S(E_f, E_i)$ , we use a computer to select at random systems which contribute to  $\mathcal{R}_S$ , statistically weighted according to the magnitude of the integrand  $\rho_e \vec{v} \cdot \vec{n}$ . The trajectories of these systems are then integrated numerically both for-

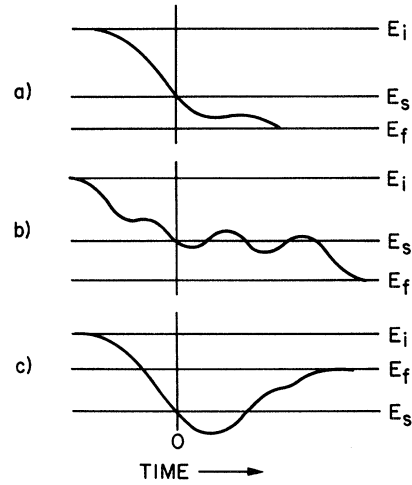


FIG. 1. Qualitative behavior of atom energy as a function of time during different types of collisions.

ward and backward in time to their final and initial configurations. A record is also kept of the number of times the trajectories cross the surface  $E_1 = E_S$ . These trajectories are then sorted according to their initial and final energies  $E_i$  and  $E_f$ . Moreover, their contributions to the rates must be divided by the number of times they cross  $E_1 = E_S$  in the downward direction. This is because each time a trajectory crosses this surface in the downward direction, it contributes to the population from which we sample (and also to the rate integral) so that in the limit of an infinite sample the  $j$ th trajectory will have been sampled  $n_j$  times ( $n_j$  = number of downward crossings). Clearly, it should be counted as a reacting atom only once. We can now estimate

$$f_S(E_f, E_i) = \sum_{j=1}^N (X_j/n_j) / N(\Delta E)^2, \quad (\text{II. 3})$$

where  $N$  is the number of trajectories sampled on the surface  $E_1 = E_S$ ,  $\Delta E$  is an arbitrary energy interval and

$$X_j = \begin{cases} 1, & \text{if the initial and final energies are} \\ & \text{within } \frac{1}{2} \Delta E \text{ of } E_i \text{ and } E_f, \text{ respectively,} \\ 0, & \text{otherwise.} \end{cases} \quad (\text{II. 4})$$

That is, we sum  $1/n_j$  over only those trajectories which contribute to  $R(E_f, E_i)$ .

The total equilibrium de-excitation rate across  $E_S$  is

$$R(E_S) = \int_{-\infty}^{E_S} dE_f \int_{E_S}^{\infty} dE_i R(E_f, E_i). \quad (\text{II. 5})$$

Substituting (2) and (3) into (5), we obtain

$$R(E_S) = f_S \mathcal{R}_S, \quad (\text{II. 6})$$

$$\text{where } f_S = \frac{1}{N} \sum_{j=1}^N (\phi_j / n_j) \quad (\text{II. 7})$$

is the fraction of trajectories leading to de-excitation and

$$\begin{aligned} \phi_j &= 1, & \text{for trajectories with } E_i > E_S > E_f, \\ &= 0, & \text{otherwise.} \end{aligned} \quad (\text{II. 8})$$

For any  $E_S$ ,  $R(E_S)$  is clearly an upper bound to the rate at which ions and electrons recombine and by a series of collisions fall to the ground state. There is a strong minimum in the curve  $R(E_S)$  versus  $E_S$ , representing a bottleneck in this relaxation process. A reasonable first estimate of the overall recombination rate may be obtained from the value of  $R(E_S)$  at this bottleneck.<sup>11</sup> We shall see that this one-way flux rate overestimates the true rate by a factor of about 3, because of neglect of re-excitation in the cascade process.

In analyzing the data one finds that about 15% of the trajectories are "exchange collisions," in which the incident electron is captured and the bound electron ejected from the atom. An experiment measuring the de-excitation rate could not differentiate between direct and exchange collisions. Hence, we want to include both in our results, and the question of how to do this correctly arises. The situation is shown schematically in Fig. 2. The vertical axis is  $E_1$ ; the horizontal axis is  $E_2 = (\vec{p}_2^2/2m) - e^2/r_2$ . Note that the center-of-mass energy  $H = E_1 + E_2 + e^2/|\vec{r}_2 - \vec{r}_1|$  and that for  $t \rightarrow \pm\infty$ ,  $|\vec{r}_2 - \vec{r}_1| \rightarrow \infty$ . Therefore, systems must start and end on the same diagonal  $E_1 + E_2$

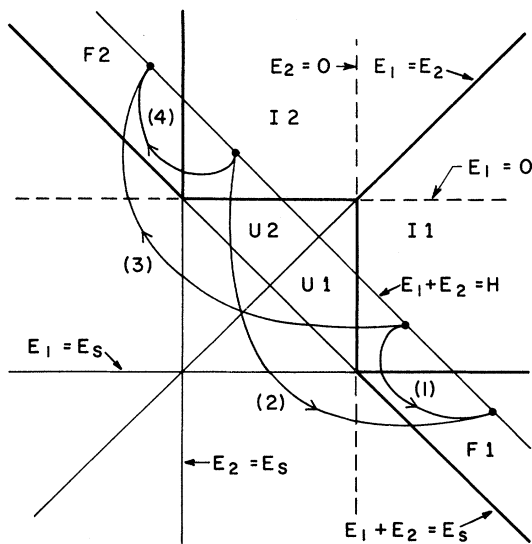


FIG. 2. Schematic diagram illustrating various states of the atom and types of trajectories encountered.

$=H$ , although they may wander to the left of that line during a collision. We are interested in initial states (denoted  $I$ ) which have one free electron ( $E > 0$ ) and one electron (bound or free) with  $E > E_S$ , and final states (denoted  $F$ ) which have one free electron ( $E > 0$ ) and one electron bound with  $E < E_S$ . The regions designated  $U$  correspond to negative ions which are unstable and which consequently cannot be terminal states. The remaining region is not allowed as a final state because of the energy conservation condition  $E_{1i} + E_{2i} = E_{1f} + E_{2f} \geq E_S$ .

There are four types of contributing trajectories as shown in Fig. 2:

- (1)  $I1 \rightarrow F1$ , (3)  $I1 \rightarrow F2$ ,
- (2)  $I2 \rightarrow F1$ , (4)  $I2 \rightarrow F2$ .

(1) and (4) correspond to direct collisions: (2) and (3) to exchange collisions. Each trajectory contributes to the statistical population from which we select, whenever it crosses  $E_1 = E_S$ . We wish to count all trajectories which start in an initial zone and end in a final zone, but we wish to count each trajectory only once.

We note first that for indistinguishable particles every real trajectory appears twice in Fig. 2. This corresponds to a relabeling of the two electrons in which each trajectory is transformed into its mirror image and only one of these must be counted. Types (1) and (2) must cross  $E_1 = E_S$  and we shall count these. Types (3) and (4) may or may not cross  $E_1 = E_S$ , but they should not be counted even if they do since we have already counted (in a statistical sense) their mirror images.

#### The Variational Rate

The variational rate (II. 1) is calculated using the equilibrium phase space density

$$\begin{aligned} \rho_e &= \frac{[A^+]_e}{(2\pi M k T)^{3/2}} \frac{[e]_e^2}{(2\pi m k T)^3} \\ &\times \exp[-(H + P^2/2M)/kT], \end{aligned} \quad (\text{II. 9})$$

where  $H$  is the center-of-mass energy,  $M$  is the atomic mass,  $[e]_e$  is the equilibrium density of free electrons and  $[A^+]_e$  is the equilibrium ion density. The above form applies to bound as well as free electrons by the assumption of equilibrium, namely, that the phase space density of electrons is a constant times  $\exp(-E/kT)$ , with the same constant applying to both free and bound electrons.

The components of the phase space velocity  $\vec{v}$  are given by Hamilton's equations

$$v_i = \frac{dx_i}{dt} = \pm \frac{\partial H}{\partial \bar{x}_i}, \tag{II. 10}$$

where  $\bar{x}_i$  is the coordinate or momentum conjugate to  $x_i$ , and the + or - apply accordingly as  $x_i$  is a coordinate or a momentum. The components of the unit normal  $\vec{n}$  are given by

$$n_i = \frac{1}{|\nabla \phi|} \frac{\partial \phi}{\partial x_i} = \left| \frac{\partial h}{\partial \phi} \right| \frac{\partial \phi}{\partial x_i}, \tag{II. 11}$$

where  $\phi = E_1 - E_S = 0$  is the equation of the surface and  $dh$  is the element of length parallel to  $\vec{n}$ .

Substituting (II. 9)–(II. 11) into (II. 1) and integrating over the center-of-mass coordinates, we obtain the rate per unit volume

$$\mathcal{R}_S = \rho_0 \int_S e^{-H/kT} |\vec{v} \cdot \nabla E_1| |d\Omega/dE_1|, \tag{II. 12}$$

where  $\rho_0 = [A^+] e [e] e^2 / (2\pi mkT)^3$ , (II. 13)

$$d\Omega = dh dS = \prod_{i=1}^{12} dx_i, \tag{II. 14}$$

and  $\vec{v} \cdot \nabla E_1 = \sum_{i=1}^{12} \left( \pm \frac{\partial H}{\partial \bar{x}_i} \right) \frac{\partial E_1}{\partial x_i}$ . (II. 15)

This last expression is familiar from Hamiltonian theory in the form

$$\frac{dE_1}{dt} (\text{along a trajectory}) = [E_1, H] \text{ (Poisson bracket).}$$

The surface of integration is subject to the constraints  $H \geq E_1 = E_S$  (since we require that one electron be free before the collision) and  $\vec{v} \cdot \nabla E_1 \leq 0$  (since we are interested in de-excitation).

Using Delaunay canonical coordinates and Eq. II. 15, and taking  $p_1$  as the dependent variable in the equation for the surface  $S$ , Eq. (II. 12) may be written

$$\begin{aligned} \mathcal{R}_S = \rho_0 \int_S e^{-H/kT} (e^2/r_{12}^2) \\ \times \left( \frac{p_1}{m} \frac{\partial r_{12}}{\partial r_1} + \frac{l_1}{mr_1^2} \frac{\partial r_{12}}{\partial \omega_1} \right) \left| \frac{\partial p_1}{\partial E_1} \right| \\ \times dr_1 dl_1 d\omega_1 dm_1 d\phi_1 dp_2 dr_2 dl_2 d\omega_2 dm_2 d\phi_2, \end{aligned} \tag{II. 16}$$

where  $p$  is the radial momentum,  $r$  is the distance from the ion,  $l$  is the angular momentum,  $m$  is the  $z$ -component of  $l$ ,  $\omega$  and  $\phi$  are the angles conjugate to  $l$  and  $m$  and the subscripts 1 and 2 denote the two electrons. These coordinates correspond to those used by Keck<sup>2</sup> with his subscripts

12, 3, and 23 replaced by 1, 2, and 12, respectively.

To integrate Eq. (II. 16) it is convenient to make the change of variables  $(\omega_1, m_1, \phi_1) \rightarrow (\beta_1, \beta_2, r_{12})$  which is most easily done through the sequence of transformations:

$$dm_1 = l_1 d(\cos \chi_1), \tag{II. 17a}$$

$$d(\cos \chi_1) d\phi_1 d\omega_1 = d(\cos \alpha) d\beta_1 d\beta_2, \tag{II. 17b}$$

and  $d(\cos \alpha) = (r_{12}/r_1 r_2) dr_{12}$ , (II. 17c)

where the angles  $\chi_1, \alpha, \beta_1$  and  $\beta_2$  are shown in Fig. 3(a). Note that the triplets  $(\phi_1, \chi_1, \omega_1)$  and  $(\beta_1, \alpha, \beta_2)$  are, respectively, the Euler angles for rotation of  $(\vec{x}, \vec{z})$  into  $(\vec{r}_1, \vec{l}_1)$  and of  $(\vec{l}_1, \vec{r}_1)$  into  $(\vec{l}_2, \vec{r}_2)$ , and that the Jacobian of the transformation (II. 17b) is unity. Also note that the transformation (II. 17c) includes a constraint on  $r_{12}$ , which we write explicitly in the form of Eq. (II. 27) below and that

$$\frac{\partial r_{12}}{\partial r_1} = -\cos \theta_2 = -\frac{r_2^2 - r_1^2 - r_{12}^2}{2r_1 r_{12}} \tag{II. 18a}$$

and

$$\frac{\partial r_{12}}{\partial \omega_1} = \frac{\partial r_{12}}{\partial \alpha} \frac{\partial \alpha}{\partial \omega_1} = -r_1 \sin \theta_2 \cos \beta_1, \tag{II. 18b}$$

where the angle  $\theta_2$  is shown in Fig. 3(b). Substituting Eqs. (II. 17) and (II. 18) into (II. 16) we obtain

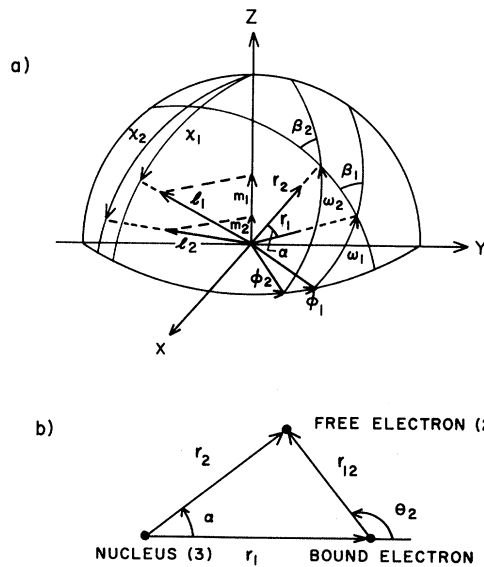


FIG. 3. Coordinates used to describe positions of the two electrons relative to the nucleus.

$$\mathcal{R}_S = \rho_0 e^2 \int_S e^{-H/kT} \quad (\text{II. 19})$$

$$\times \left( p_1 \cos \theta_2 + \frac{l_1}{r_1} \cos \beta_1 \sin \theta_2 \right) \frac{1}{|p_1|} \frac{l_1}{r_1 r_2 r_{12}} \\ \times d\phi_2 d\omega_2 d\beta_2 dm_2 dl_2 dp_2 d\beta_1 dl_1 dr_1 dr_2 dr_{12},$$

$$\text{where } p_1 = \pm [2m(E_S + e^2/r_1) - l_1^2/r_1^2]^{1/2} \quad (\text{II. 20})$$

is the radial momentum of electron 1 on the surface  $E_1 = E_S$ , and the surface of integration is limited by the constraints

$$H = E_S + \frac{p_2^2}{2m} + \frac{l_2^2}{2mr_2^2} - \frac{e^2}{r_2} + \frac{e^2}{r_{12}} \geq E_S \quad (\text{II. 21})$$

$$\text{and } p_1 \cos \theta_2 + (l_1/r_1) \cos \beta_1 \sin \theta_2 \geq 0. \quad (\text{II. 22})$$

Integrating Eq. (II. 19) over the first eight variables and summing the contributions from positive and negative  $p_1$ , we find

$$\mathcal{R}_S = \rho_0 32\pi^4 m e^2 (2mkT)^{3/2} e^{-E_S/kT} \\ \times \int e^{-V_2/kT} F(-V_2/kT) \\ \times \left( \frac{e^2}{r_1} + E_S \right) \frac{r_1 r_2}{r_{12}} dr_1 dr_2 dr_{12}, \quad (\text{II. 23})$$

$$\text{where } V_2 = e^2/r_{12} - e^2/r_2 \quad (\text{II. 24})$$

is the potential of electron 2,

$$F(x) = \int_x^\infty y^{1/2} e^{-y} dy, \quad x \geq 0; \\ = \frac{1}{2} \sqrt{\pi}, \quad x \leq 0; \quad (\text{II. 25})$$

and the integration is subject to the conditions

$$(e^2/r_1) + E_S \geq 0 \quad (\text{II. 26})$$

$$\text{and } |r_2 - r_{12}| \leq r_1 \leq r_2 + r_{12} \quad (\text{II. 27})$$

necessary for real solutions of Eqs. (II. 20) and (II. 17c), respectively.

It can now be seen that, due to the long range of the Coulomb potential, the integral in Eq. (II. 23) diverges linearly with  $r_2$ , and a cutoff condition must be chosen. We anticipate, however, that the actual reaction rate  $R(E_S)$  will be independent of the cutoff because the fraction  $f_S$  in (6) approaches zero for large  $r_2$ . The reason for this is that for distant collisions the number of crossing  $n_j$  of the critical surface tends to be large because the bound electron makes many orbits during the collision time in which it alternately gains and loses energy as illustrated in Fig. 1(b). Also there are fewer cases contributing to the sum in Eq. (II. 7) since many of the trajectories are unsuccessful in crossing the critical surface as illustrated in

Fig. 1(c).

In analyzing the data the cutoff condition

$$(r_2 + r_{12})(-E_S/e^2) \leq \beta \quad (\text{II. 28})$$

was used. This gave a partial rate

$$R(E_S, \beta) = f_S(\beta) \mathcal{R}_S(\beta) \quad (\text{II. 29})$$

which had the same  $\beta$  dependence independent of the values of  $E_S$  or  $kT$ . (See Sec. III, Fig. 4.)

To carry out the remaining integration of Eq. (II. 23) it is convenient to introduce the dimensionless variables

$$\rho_\pm = (r_2 \pm r_{12})(-E_S/e^2), \quad \text{and } \epsilon_S = E_S/kT. \quad (\text{II. 30})$$

The integration over  $r_1$  can be carried out explicitly and the result expressed in the form

$$\mathcal{R}_S(\beta) = R_0 e^{-\epsilon_S} (-\epsilon_S)^{-3} \phi_S(\beta), \quad (\text{II. 31})$$

where

$$R_0 = [A^+] e [e] e^2 (kT/m)^{1/2} (e^2/kT)^5 \\ = 2.59 \times 10^{-27} \frac{[A^+] e [e]^2}{[kT(eV)]^{9/2}} \text{ cm}^{-3} \text{ sec}^{-1} \quad (\text{II. 32})$$

is a characteristic three-body collision rate based on the Thompson radius ( $e^2/kT$ ), and

$$\phi_S(\beta) = 2\pi\sqrt{2} \int_0^\beta \int_{-\rho}^{\rho} e^{-u_2} F(-u_2) \\ \times G(\rho_+, \rho_-) \frac{\rho_+ + \rho_-}{\rho_+ - \rho_-} d\rho_- d\rho_+, \quad (\text{II. 33})$$

$$\text{in which } G(\rho_+, \rho_-) = 2\rho_+ - \rho_+^2 - 2\rho_- + \rho_-^2, \quad (\text{II. 34})$$

$$\rho_+ = \min(\rho_+, 1), \quad (\text{II. 35})$$

and

$$u_2 = V_2/kT = 4\epsilon_S \rho_- / (\rho_-^2 - \rho_+^2). \quad (\text{II. 36})$$

In general, the integral in Eq. (II. 33) must be evaluated numerically; however, for  $\beta > (-\epsilon_S)^{1/2} > 1$ , which is the range of interest in the present study, it may be evaluated approximately and we obtain

$$\phi_S(\beta) \approx \frac{1}{3} (2\pi)^{3/2} [\beta - \frac{1}{2} (-\epsilon_S)^{1/2}]. \quad (\text{II. 37})$$

This expression has been checked numerically for the range  $1 \leq (-\epsilon_S) \leq 6$ , and is accurate to 20%

for  $\beta \geq \sqrt{-\epsilon_s}$  and to better than 5% for  $\beta \geq 2\sqrt{-\epsilon_s}$ . In the following work however, we have used the numerically calculated results.

Monte Carlo Calculations

We have selected our trajectories with a weight proportional to the integrand in Eq. (II. 19). This gives us the maximum statistical accuracy in the regions which make the largest *a priori* contribution to the rate as well as allowing us to obtain  $f_S(\beta)$  without further weighting. Our procedure is based on the following theorems, proof of which may be found in standard texts on statistics:

Theorem 1: Given a function  $f(x)$  defined on  $[a, b]$ . Select random numbers  $X$  from a population uniformly distributed on the interval  $[0, 1]$ . Choose  $x$  by solving

$$\int_a^x f(x')dx' / \int_a^b f(x')dx' = X. \quad (II. 38)$$

Then the  $x$ 's selected in this manner will be distributed according to the weighting function  $f(x)$ .

Theorem 2: Given  $g(x_1, \dots, x_n)$ , ( $n \geq 2$ ), defined on  $\prod_{i=1}^n [a_i, b_i]$ , and given that  $(x_1, \dots, x_{n-1})$  have been selected according to the weighting function

$$h(x_1, \dots, x_{n-1}) = \int_a^b g(x_1, \dots, x_{n-1}, x_n) dx_n;$$

define  $f(x_n) = g(x_1, \dots, x_n)$  using the given values of  $(x_1, \dots, x_{n-1})$ , and select  $x_n$  according to  $f(x_n)$  using the preceding theorem. Then points  $(x_1, \dots, x_n)$  selected in this way will be distributed according to the weighting function  $g(x_1, \dots, x_n)$ .

To apply these theorems we perform the innermost integrations first and the corresponding selections last. Thus, the first coordinates to be chosen are  $\rho_+$  and  $\rho_-$ . These were selected using the integrand in Eq. (II. 33) as a bivariate weighting function. The general procedure was as follows: Let  $x$  and  $y$  be arbitrary variables to be selected from within a rectangle  $x_1 < x < x_2$ ,  $y_1 < y < y_2$ , and  $f(x, y)$  be the distribution function. We divide the  $x$  domain and the  $y$  domain each into 30 intervals, thus getting 900 subrectangles which we order in some arbitrary way. Three random numbers are generated. The first ( $X_1$ ) is used to select a subrectangle according to the discrete distribution function  $f_i =$  value of  $f(x, y)$  at the center of the  $i$ th subrectangle; i. e., subrectangle  $n$  is selected when

$$\sum_{i=1}^{n-1} f_i / \sum_{i=1}^{900} f_i \leq X_1 \leq \sum_{i=1}^n f_i / \sum_{i=1}^{900} f_i. \quad (II.39)$$

The second ( $X_2$ ) is used to select a particular  $x$  within that subrectangle by assuming that all val-

ues of  $x$  within the subrectangle are equally probable. The third ( $X_3$ ) selects  $y$ , similarly. This procedure is equivalent to using a "step-function" distribution function which has a constant value  $f_i$  over the  $i$ th subrectangle. The resultant distribution will approximate  $f(x, y)$  to the extent that  $f(x, y)$  does not vary greatly over any subrectangle. We are at liberty to choose the variables  $x$  and  $y$  as simple functions of  $\rho_+$  and  $\rho_-$  in such a way as to flatten  $f(x, y)$  as much as possible, especially near the ridge at  $\rho_- = 0$  where most of the distribution occurs. Note that  $f(x, y)$  includes not only the original  $\rho_+$ ,  $\rho_-$  integrand, but also the Jacobian of the transformation to  $x, y$ . In our program we used

$$\rho_+ = x, \quad 0 \leq x \leq 1; \quad (II.40a)$$

$$= (\beta - 1)(x - 1) + 1, \quad 1 \leq x \leq 2;$$

$$\text{and } \rho_- = x\phi(y), \quad 0 \leq x \leq 1; \quad (II.40b)$$

$$= \phi(y), \quad 1 \leq x \leq 2;$$

where

$$\phi(y) = \text{sgn}(y)[1 - (1 - |y|)^{1/2}], \quad -1 \leq y \leq 1.$$

III. RESULTS

Our results are based on an analysis of 7800 individual trajectories distributed as shown in Table I. Error bars on the figures represent a statistical  $1/\sqrt{N}$  relative uncertainty.

Figure 4 shows that dependence of the results

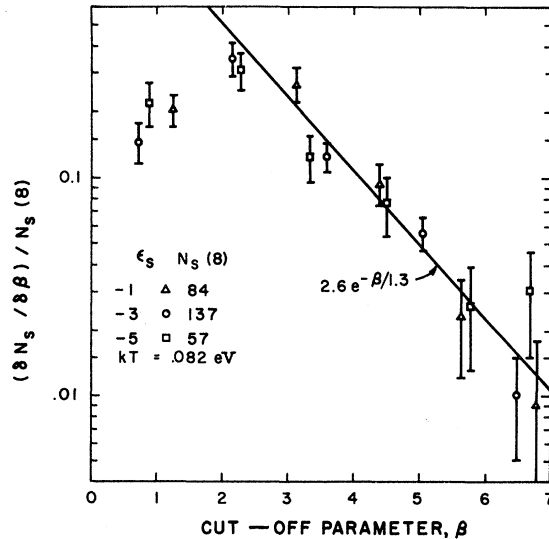


FIG. 4. Rate of increase in the number of successful trajectories divided by the total number of successful trajectories,  $(\delta N_s / \delta \beta) / N_s(\beta)$ , as a function of the cutoff parameter  $\beta$ . The maximum value of  $\beta$  was 8.

TABLE I. Number of trajectories analyzed at each condition investigated.

$\frac{-E_s}{kT}$	$kT$ (eV)			
	0.027	0.082	0.27	0.82
1		500		
2		500		
3	500	2900	300	300
4		1000		
5		1000		
6		1000		

on the value of the cutoff parameter  $\beta$  for a temperature  $kT=0.082$  eV and the surfaces  $\epsilon_s = -1$ ,  $-3$ , and  $-5$ . The term  $\delta N_s/\delta\beta$  is the rate of increase in the number of successful trajectories with  $\beta$  and  $N(\beta)$  is the total number of trajectories sampled with  $\rho_+ \leq \beta$ . Note that since we have sampled in proportion to the integrand in Eq. (II.33)

$$N_s(\beta) = N(\beta) f_s(\beta) \propto \phi_s(\beta) f_s(\beta) \propto R(E_s, \beta), \quad (\text{III.1})$$

where  $R(E_s, \beta)$  is given by Eq. (II.29) and  $f_s(\beta)$  by the analog of Eq. (II.7)

$$f_s(\beta) = \frac{N(\beta)}{\sum_{j=1}^N [\phi_j(\beta)/n_j(\beta)]/N(\beta)}, \quad (\text{III.2})$$

where  $\phi_j(\beta) = 1$ , if  $E_i > E_s > E_f$  and  $\rho_+ \leq \beta$ ;  
 $= 0$ , otherwise;

and  $n_j(\beta)$  is the number of downward crossing for which  $\rho_+ \leq \beta$ .

It can be seen from Fig. 4 that for  $\beta > 3$

$$(\delta N_s/\delta\beta)/N(8) \approx 2.6 e^{-\beta/1.3} \quad (\text{III.4})$$

with no significant dependence on  $\epsilon_s$ . Extrapolating to  $\beta = \infty$  we find from Eqs. (III.1) and (III.4) that

$$\begin{aligned} R(E_s) &= R(E_s, \infty) \\ &= (1 + 2.6 \int_8^\infty e^{-\beta/1.3} d\beta) R(E_s, 8) \\ &= 1.01 R(E_s, 8) \end{aligned} \quad (\text{III.5})$$

which shows that the contribution of successful trajectories from the range  $\beta > 8$  is negligible compared to our statistical errors.

Figure 5 shows the fraction  $f_s(\beta)$  of successful

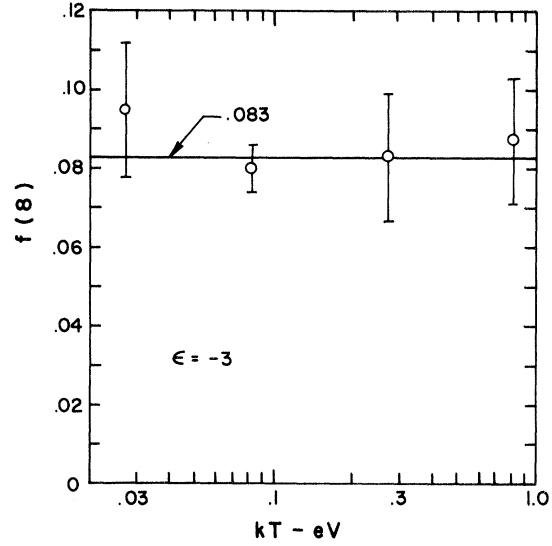


FIG. 5. Fraction of successful trajectories  $f_s(8)$  as a function of temperature.

trajectories as a function of temperature for  $\epsilon_s = -3$  and  $\beta = 8$ . Within the statistical errors,  $f_s(8)$  is independent of temperature in the range  $0.03 \leq kT \leq 0.8$  eV and has a mean value of  $0.083 \pm 0.005$ . This means that only one out of every 12 trajectory-crossings represents a permanent crossing of surface  $E_s$  and suggests that adiabatic collisions (in which a single collision includes many crossings of the surface) are very important as we anticipated.

Figure 6 shows the dependence of the combination of factors  $\phi_s(\beta) f_s(\beta)$  on  $\epsilon_s$  for  $\beta = 8$  and  $kT = 0.082$  eV. It is this combination of factors which appears in the flux rate  $R(E_s, \beta)$  and which retains the same dependence on  $\epsilon_s$  as  $\beta \rightarrow \infty$ . For the range  $1 \leq (-\epsilon_s) \leq 6$ , a least-squares fit of the data gives

$$\phi_s(8) f_s(8) = 7.8 (-\epsilon_s)^{-0.83}. \quad (\text{III.6})$$

Combining the numerical results of Figs. 4-6 with Eqs. (III.29), and (III.31) we find the equilibrium crossing rate

$$R(\epsilon_s) = 7.8 R_0 e^{-\epsilon_s} (-\epsilon_s)^{-3.83} \quad (\text{III.7})$$

with an error of approximately  $\pm 5\%$  based on the statistical  $1/\sqrt{N}$  deviation of all the data. Note that  $R(\epsilon_s)$  has a relatively strong minimum at  $\epsilon_s = -3.83$  and approaches infinity at the ionization limit  $\epsilon_s = 0$ .

The differential reaction rate

$$R(\epsilon_f, \epsilon_i) = R(E_f, E_i) (kT)^2 \quad (\text{III.8})$$

is shown in Fig. 7 as a function of  $\epsilon_i$  and  $\epsilon_f$  for  $\beta = 8$  and  $kT = 0.082$  eV. The figures in the boxes

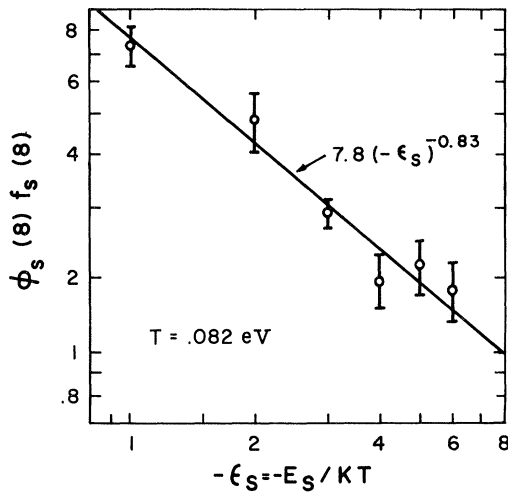


FIG. 6. Dependence of the combination of factors  $\phi_s(8) f_s(8)$  on energy of surface  $\epsilon_s$  on which trajectories were sampled.

are the mean value of  $R(\epsilon_f, \epsilon_i)/R_0$  for the box. Because of the sampling technique employed each value of  $\epsilon_s$  used in the calculations gives data in a quadrant that touches the diagonal  $\epsilon_i = \epsilon_f$  at a value of  $(\epsilon_i + \epsilon_f)/2 = \bar{\epsilon} = \epsilon_s$ . Data in overlapping quadrants agreed within the statistical errors and were averaged to obtain the results shown. To avoid crowding the figure, errors are not shown but are about  $\pm 15\%$  near the diagonal and increase to  $\pm 30\%$  for  $\epsilon_i - \epsilon_f = 6$ . The results shown were calculated for  $\epsilon_i > \epsilon_f$ ; however since  $R(\epsilon_f, \epsilon_i)$  is symmetric in  $\epsilon_f$  and  $\epsilon_i$ , the values for  $\epsilon_i < \epsilon_f$  may be obtained by reflection in the diagonal  $\epsilon_i = \epsilon_f$ . It can be seen that the complete function has a sharp ridge along  $\epsilon_i = \epsilon_f$  which corresponds to zero energy transfer and a saddle point at  $\epsilon_s \approx -4$  which corresponds to the minimum in  $R(\epsilon_s)$  previously mentioned.

An alternative presentation of the data for  $R(\epsilon_f, \epsilon_i)$  is given in Fig. 8 which shows a plot of  $R(\epsilon_f, \epsilon_i)/(R_0 e^{-\epsilon_i})$  as a function of  $\epsilon_f$  for various values of the energy transfer  $\Delta\epsilon = \epsilon_i - \epsilon_f$ . Representative statistical errors are shown on several of the points. It can be seen that within these errors the data are essentially independent of  $\Delta\epsilon$  over the range  $0.5 \leq \Delta\epsilon \leq 6$  and that for  $\epsilon_i > \epsilon_f$

$$R(\epsilon_f, \epsilon_i) = 30 R_0 e^{-\epsilon_i} (-\epsilon_f)^{-4.83}$$

$$= 7.8 \times 10^{-26} [A^+]_e [e]_e^2 \quad (III.9)$$

$$\times [kT(\text{eV})]^{-\frac{9}{2}} e^{-\epsilon_i} (-\epsilon_f)^{-4.83} \text{cm}^{-3} \text{sec}^{-1}$$

This function is shown as a contour plot in Fig. 9 and fits the data in Fig. 7 well within the statistical

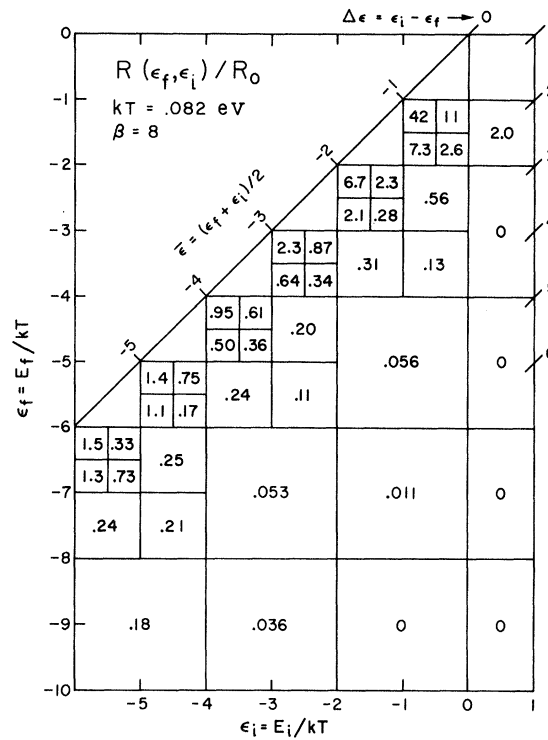


FIG. 7. Differential equilibrium reaction rate  $R(\epsilon_f, \epsilon_i)$  for transitions from initial states of energy  $\epsilon_i$  to the final states of energy  $\epsilon_f$ . Numbers in boxes are averages over box. Statistical errors vary from  $\pm 15\%$  near  $\Delta\epsilon = 0$  to  $\pm 30\%$  for  $\Delta\epsilon = 6$ .

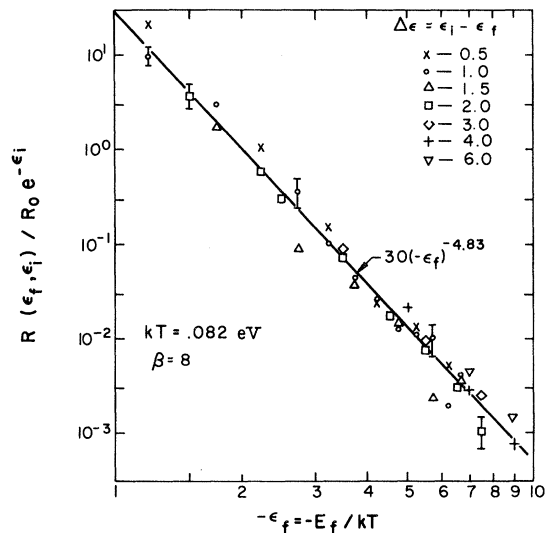


FIG. 8. Plot of  $R(\epsilon_f, \epsilon_i) e^{\epsilon_i}$  as a function of the final energy  $\epsilon_f$ . Errors shown are typical of points in their neighborhood. Note that within the statistical accuracy  $R(\epsilon_f, \epsilon_i) e^{\epsilon_i}$  is independent of the energy transfer  $\Delta\epsilon$ .

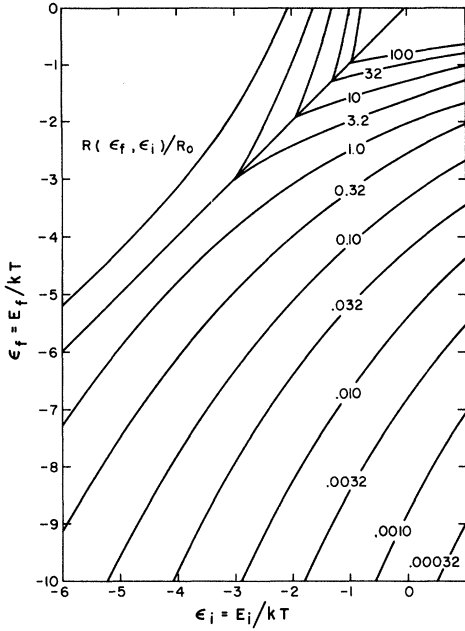


FIG. 9. Contour plot of  $R(\epsilon_f, \epsilon_i)$  calculated from Eq. (III.9) which represents a smooth fit to the data in Figs. 7 and 8.

accuracy. In fact, a "Chi-Square" test indicates that the chance of obtaining a better fit is less than 20%. Note that substitution of Eq. (III.9) into Eq. (II.5) yields exactly Eq. (III.7) as required.

Considering the range of condition spanned, it is remarkable that such a simple function fits the data so well. Whether this has any physical significance is not clear. However, it is interesting to note that our expression for  $R(\epsilon_f, \epsilon_i)$  is very nearly proportional to the Boltzmann factor for the upper state times the square of the phase volume per unit energy for the lower state. Since we should expect  $R(\epsilon_f, \epsilon_i)$  to be proportional to the product of the initial- and final-level densities, this suggests that the initial and final states are at least approximately restricted to the same volume in phase space.

The rate constant for transition from  $\epsilon_i$  to  $\epsilon_f$  can be obtained from the definition

$$k(\epsilon_f, \epsilon_i) = R(\epsilon_f, \epsilon_i) / [e]_e (d[A] / d\epsilon_i)_e, \quad (\text{III.10})$$

where

$$\left( \frac{d[A]}{d\epsilon} \right)_e = [A^+]_e [e]_e \frac{\pi^{3/2}}{2} \left( \frac{e^2}{kT} \right)^3 \frac{e^{-\epsilon}}{(-\epsilon)^{5/2}} \quad (\text{III.11})$$

is the equilibrium density of atoms per unit  $\epsilon$  obtained by requiring that the bound electrons be in equilibrium with the free electrons. Substituting Eq. (III.9) into Eq. (III.10) we obtain

$$k(\epsilon_f, \epsilon_i) = 11 \cdot k_0 \begin{cases} (-\epsilon_f)^{-4.83} (-\epsilon_i)^{2.5}, & \epsilon_i > \epsilon_f; \\ (-\epsilon_i)^{-2.33} e^{-(\epsilon_f - \epsilon_i)}, & \epsilon_i < \epsilon_f; \end{cases} \quad (\text{III.12})$$

where

$$k_0 = \left( \frac{kT}{m} \right)^{\frac{1}{2}} \left( \frac{e^2}{kT} \right)^2 = 8.7 \times 10^{-7} [kT(\text{eV})]^{-3/2} \text{ cm}^3 \text{ sec}^{-1} \quad (\text{III.13})$$

is a characteristic binary-collision rate constant based on the Thompson radius. This expression is independent of the density of atoms in the initial state, but assumes that the free electrons are maintained in a Boltzmann distribution. This is the case in many nonequilibrium situations of interest.

The total collision rate  $k(\epsilon_i)$  obtained from Eq. (III.12) is

$$k(\epsilon_i) = \int_{-\infty}^{\infty} k(\epsilon_f, \epsilon_i) d\epsilon_f = 11 k_0 (1 - \epsilon_i / 3.83) (-\epsilon_i)^{-2.33}, \quad (\text{III.14})$$

and the mean-square energy transfer is

$$\langle \Delta\epsilon^2 \rangle = \int_{-\infty}^{\infty} (\epsilon_f - \epsilon_i)^2 k(\epsilon_f, \epsilon_i) d\epsilon_f / k(\epsilon_i) = 2[1 + 0.050(-\epsilon_i)^3] / (1 - \epsilon_i / 3.83) \quad (\text{III.15})$$

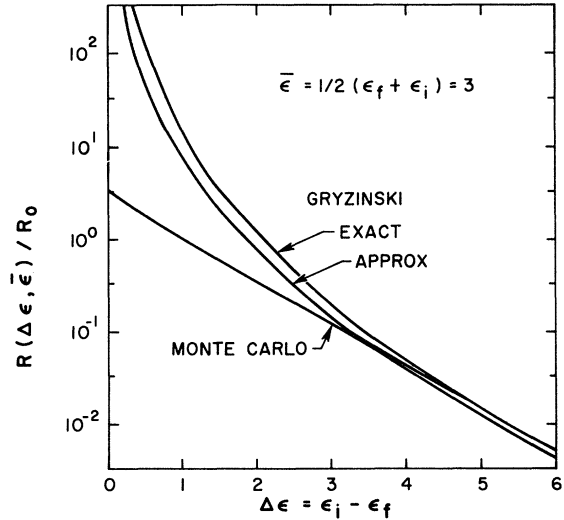


FIG. 10. Comparison of differential equilibrium re-action rate  $R(\Delta\epsilon, \bar{\epsilon})$  obtained in the present Monte Carlo calculation with results obtained by Gryzinski using the impulse approximation. Note that the impulse approximation which diverges as  $(\Delta\epsilon)^{-3}$  overestimates the probability of small energy transfer by a large factor. This is the result of treating adiabatic collisions in an impulse approximation.

which is relatively large. This makes the diffusion approximation used by Gurevich and Pit-

aevskii<sup>8</sup> in their treatment of collisional cascading somewhat questionable.

#### Comparison with Impulse Approximation

To compare our results with those obtained by Gryzinski<sup>5,6</sup> using the impulse approximation, we have computed the equilibrium transition rate from the expression

$$R(E_f, E_i) = \int_0^\infty \int_{\Delta E}^\infty \rho_2(T_2) \rho_1(E_i, T_1) \sigma(\Delta E, T_1, T_2) v_2 dT_1 dT_2, \quad (\text{III. 16})$$

where  $\Delta E = E_i - E_f \geq 0$  is the energy lost by the atom

$$\rho_2(T_2) = \frac{[e]_e}{(2\pi m k T)^{3/2}} \left( \frac{4\pi p_2^2 dp_2}{dT_2} \right) e^{-T_2/kT} = \frac{[e]_e 8\pi m T_2}{(2\pi m k T)^{3/2} v_2} e^{-T_2/kT} \quad (\text{III. 17})$$

is the equilibrium density per unit energy of free electrons with kinetic energy  $T_2 = (1/2)mv_2^2$ ,

$$\rho_1(E_i, T_1) = \frac{[e]_e [A^+]_e}{(2\pi m k T)^{3/2}} \left( \frac{4\pi r_1^2 dr_1}{dE_i} \right) \frac{4\pi p_1^2 dp_1}{dT_1} e^{-E_i/kT} = \frac{32\pi^2 m T_1}{(T_1 - E_i)^4 v_1} e^{-E_i/kT} \quad (\text{III. 18})$$

is the equilibrium density per (unit energy)<sup>2</sup> of bound electrons with total energy  $E_i$  and kinetic energy  $T_1 = (1/2)mv_1^2$  and  $\sigma(\Delta E, T_1, T_2)$  is the cross section for electron-electron scattering with energy transfer  $\Delta E$ .

Equation (III. 16) has been integrated numerically using both exact and approximate cross sections given by Gryzinski and some typical results are shown in Fig. 10. The curve labeled "exact" was obtained using the expression<sup>6</sup>

$$\sigma_{\text{ex}}(\Delta E, T_1, T_2) = \frac{4\pi e^4 T_1}{3(\Delta E)^3 T_2} \begin{cases} (1 + 3\Delta E/T^2)(T_2/T_1)^{3/2}, & 0 \leq \Delta E \leq T_1 - T_2 \\ (1 - \Delta E/4T_1)(1 - \Delta E/T_1)^{1/2}, & T_1 - T_2 \leq \Delta E \leq T_1 \end{cases} \quad (\text{III. 19})$$

For large values of  $\Delta E$  the "exact" curve is asymptotic to our results within the statistical errors. This is to be expected since for large energy transfers the collisions tend to be impulsive and recrossing of the critical surface is negligible. However, for small energy transfer the collisions tend to be adiabatic, and the impulse approximation leads to a gross overestimate of the reaction rate.

The curve labeled "approx" was computed using the expression<sup>5</sup>

$$\sigma_{\text{ap}}(\Delta E, T_1, T_2) = [4\pi e^4 T_1 / 3(\Delta E)^3 T_2] [T_2 / (T_1 + T_2)]^{3/2} \times \begin{cases} 1 + 3\Delta E/4T_2 - 3\Delta E/4T_1, & 0 \leq \Delta E \leq T_1 - T_2; \\ [1 - \Delta E/4T_1 + \Delta E/4T_2 + (\Delta E)^2/2T_1 T_2] (1 - \Delta E/T_1)^{1/2} (1 + \Delta E/T_2)^{1/2}, & T_1 - T_2 \leq \Delta E \leq T_1. \end{cases} \quad (\text{III. 20})$$

The derivation of this cross section involves the approximation  $\vec{v}_1 \cdot \vec{v}_2 = 0$  which Gryzinski suggests as a method of reducing the contribution from adiabatic collisions. Although Eq. (III.20) leads to a slight reduction in the magnitude of the reaction rate, it does not change the shape of the curve significantly and, therefore, does not really accomplish the purpose intended.

On the basis of the comparison in Fig. 10, we conclude that while the impulse approximation is reasonable for large energy transfer, it is not at all satisfactory for small energy transfer. It follows that, for closely spaced levels such as those near the ionization limit of an atom, cutting off the classical cross section at the quantum-mechanical level spacing is incorrect and that a more reasonable procedure would be to cut-off when the adiabaticity parameter  $\omega\tau$  becomes of order unity. This is particularly relevant to calculations of collisional-radiative recombination such as those of Bates, Kingston, and McWhirter<sup>7</sup> in which a cutoff at the level spacing is tacitly assumed. The reason such calculations give moderately good agreement with experiments is due to the fact that the "diffusion" of atoms up and down the energy ladder is basically governed by the second moment of the energy transfer per collision,<sup>4</sup> and this is much less sensitive to the cutoff than the cross section itself.

It may be noted in concluding this discussion that the same divergence in the cross section for small energy transfer occurs for collisions of astronomical bodies, and that invoking a cutoff at the level spacing in this case would obviously be ridiculous.

#### IV. STEADY-STATE REACTION RATE

At high electron concentrations and low temperatures radiative processes are negligible, and ionization and recombination proceeds via a collisional cascade in which the atoms are successively excited and de-excited by electron impact. Furthermore, the rate limiting step in this cascade usually occurs within a few  $kT$  of the dissociation limit where the level density is high and collisions may be treated classically. Under these conditions the cascade may be described by the master equation.

$$\begin{aligned} \frac{\partial N(\epsilon, t)}{\partial t} = [e] \int_{-\delta}^{\infty} d\epsilon' \\ \times [k(\epsilon, \epsilon')N(\epsilon', t) - k(\epsilon', \epsilon)N(\epsilon, t)], \end{aligned} \quad (\text{IV. 1})$$

where  $N(\epsilon, t) = d[A]/d\epsilon$  is the density of atoms per unit  $\epsilon$  with energy  $\epsilon$ ,  $k(\epsilon', \epsilon)$  is the transition-rate constant defined by Eq. (III. 10) and  $\delta$  is the ionization energy in units of  $kT$ . Making the substitution

$$X(\epsilon, t) = N(\epsilon, t)/N_e(\epsilon) \quad (\text{IV. 2})$$

in Eq. (IV. 1), we obtain

$$\begin{aligned} \frac{\partial N(\epsilon, t)}{\partial t} = \frac{[e]}{[e]_e} \int_{-\delta}^{\infty} d\epsilon' R(\epsilon', \epsilon) \\ \times [X(\epsilon', t) - X(\epsilon, t)], \end{aligned} \quad (\text{IV. 3})$$

where  $R(\epsilon', \epsilon) = k(\epsilon', \epsilon)N_e(\epsilon)[e]_e$  is the equilibrium transition rate.

For a separable kernel of the form

$$\begin{aligned} R(\epsilon', \epsilon) = r_1(\epsilon')r_2(\epsilon), \quad \epsilon' \leq \epsilon; \\ = r_1(\epsilon)r_2(\epsilon'), \quad \epsilon \leq \epsilon'; \end{aligned} \quad (\text{IV. 4})$$

the steady-state solution of Eq. (IV. 3) which satisfies the condition that the free electrons have a Boltzmann distribution,

$$X(\epsilon, t) = \frac{[e][A^+]}{[e]_e[A^+]_e} \equiv X(\infty, t), \quad \epsilon > 0; \quad (\text{IV. 5})$$

is  $X(\epsilon, t) = X(\infty, t)$

$$+ [X(-\delta, t) - X(\infty, t)] \chi(\epsilon), \quad \epsilon < 0; \quad (\text{IV. 6})$$

$$\begin{aligned} \text{where } \chi(\epsilon) = \left( \int_{\epsilon}^0 \frac{Wd\epsilon'}{Z^2} + \frac{r_2(0)}{r_+(0)Z(0)} \right) \\ \times \left( \int_{-\delta}^0 \frac{Wd\epsilon'}{Z^2} + \frac{r_2(0)}{r_+(0)Z(0)} \right)^{-1} \end{aligned} \quad (\text{IV. 7})$$

is the energy distribution function,

$$W(\epsilon) = r_2(\epsilon) \frac{dr_1(\epsilon)}{d\epsilon} - r_1(\epsilon) \frac{dr_2(\epsilon)}{d\epsilon} \quad (\text{IV. 8})$$

is the Wronskian of  $r_1$  and  $r_2$ ,

$$Z(\epsilon) = \int_{-\delta}^{\infty} R(\epsilon', \epsilon) d\epsilon' = r_2(\epsilon)r_-(\epsilon) + r_1(\epsilon)r_+(\epsilon) \quad (\text{IV. 9})$$

is the equilibrium collision rate per unit energy,

$$r_-(\epsilon) = \int_{-\delta}^{\epsilon} r_1(\epsilon') d\epsilon' \quad (\text{IV. 10a})$$

$$\text{and } r_+(\epsilon) = \int_{\epsilon}^{\infty} r_2(\epsilon') d\epsilon'. \quad (\text{IV. 10b})$$

In general, the factor  $W/Z^2$  in Eq. (IV. 7) has a relatively strong maximum at an energy  $\epsilon_b$  in the vicinity of the ionization limit so that for  $\epsilon < \epsilon_b$ ,  $\chi(\epsilon) \approx 1$  while for  $\epsilon > \epsilon_b$ ,  $\chi(\epsilon) \approx 0$ . Thus,  $\epsilon_b$  may be interpreted as the location of the "bottle-neck" on the energy ladder which effectively divides atoms from ion-electron pairs.

Substituting Eq. (IV. 7) into Eq. (IV. 3) and integrating<sup>12</sup> from  $-\delta$  to  $\epsilon_b$ , we obtain the familiar phenomenological rate equation

$$\frac{\partial [A]}{\partial t} = a[e][A^+] - aK_e[A], \quad (\text{IV. 11})$$

where  $K_e = [e]_e[A^+]_e/[A]_e$  is the Saha equilibrium constant.

$$\begin{aligned} a = \frac{[e] \left( 1 - \frac{r_-(\epsilon_b)r_2(0)}{Z(0)} - \frac{r_+(\epsilon_b)r_1(-\delta)}{Z(0)} \right)}{[A^+]_e [e]_e^2 \left( \int_{-\delta}^0 \frac{W}{Z^2} d\epsilon + \frac{r_2(0)}{r_+(0)Z(0)} \right)} \end{aligned} \quad (\text{IV. 12})$$

is the steady-state recombination-rate constant and we have used the approximation

$$[A] = \int_{-\delta}^{\epsilon_b} N_e(\epsilon) X(\epsilon, t) d\epsilon \approx X(-\delta, t) [A]_e, \quad (\text{IV. 13})$$

which is valid for

$$[d\chi(\epsilon)/d\epsilon]_{-\delta} \ll 1. \quad (\text{IV. 14})$$

Using the expression in Eq. (III. 9) for the transition kernel, we find from Eqs. (IV. 8) and (IV. 9)

$$\frac{W}{Z^2} = \frac{(3.83)^2(4.83 - \epsilon)(-\epsilon)^{3.83} e^{-\epsilon}}{30R_0(3.83 - \epsilon)^2}. \quad (\text{IV. 15})$$

Substituting Eq. (IV. 15) into Eq. (IV. 7) and carrying out approximate integration (see Appendix A) gives the distribution function

$$\chi(\epsilon) = \{3.3, -\epsilon\}! / \{3.3, \delta\}!, \quad (\text{IV. 16})$$

$$\text{where } \{p, x\}! = \int_0^x y^p e^{-y} dy = \gamma(p+1, x) \quad (\text{IV. 17})$$

is the incomplete factorial, and we have used the boundary condition  $Z(0) = \infty$ . The corresponding recombination-rate constant obtained from Eq. (IV. 12) is

$$\begin{aligned} a &= 0.76 R_0 [e] / [A^+]_e [e]_e^2 \\ &= 2.0 \times 10^{-27} [e] [kT(\text{eV})]^{-9/2} \text{ cm}^3 \text{ sec}^{-1}, \end{aligned} \quad (\text{IV. 18})$$

where we have assumed that  $\delta \geq 10$ . The estimated statistical accuracy of this result in the range  $0.03 \leq kT \leq 1$  eV is  $\pm 20\%$ . This value of  $a$  is roughly one-third the one-way flux-rate constant

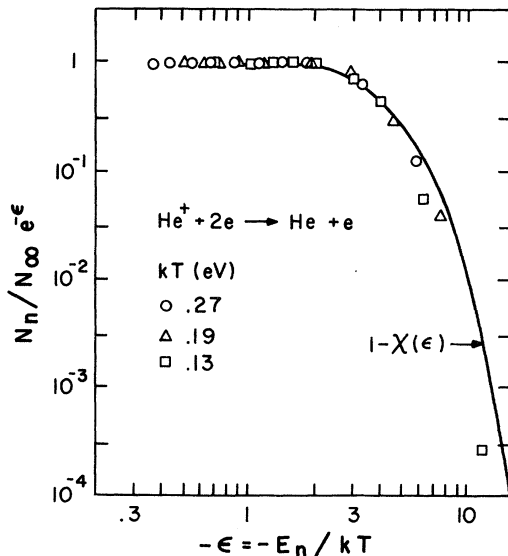


FIG. 11. Comparison of theoretical population distribution,  $1 - \chi(\epsilon)$ , for a recombining He plasma with experimental measurements of Hinnov and Hirschberg.<sup>10</sup> The smaller observed populations at lower energies may be attributed to the effect of radiative depopulation of these states.

$$\begin{aligned} a_1 &= R(-3.83)[e]/[A^+]_e [e]_e^2 \\ &= 2.1 R_0 [e]/[A^+]_e [e]_e^2 \end{aligned}$$

obtained by evaluating (III. 7) at the minimum at  $\epsilon_S = 3.83$ . As previously mentioned  $a_1$  has been used<sup>9</sup> to obtain a rough estimate of  $a$ , but does not take into account re-excitations which occur during the collisional cascading.

#### Comparison with Experiment

Measurements of the population distribution in a recombining helium plasma have been made by Hinnov and Hirschberg,<sup>13</sup> and their results are compared with the theoretical prediction in Fig. 11. In the neighborhood of the "bottleneck" at  $\epsilon = -3.3$ , the theoretical curve agrees well with the experimental points. However, at lower energies the measured populations are somewhat less than the theoretical prediction. As we shall see later this is probably the result of depopulation of the lower levels by radiation.

Measurements of the recombination rate coefficient under collision-limited conditions have been made for H,<sup>13</sup> He,<sup>13,14</sup> and Cs.<sup>15-18</sup> The experimental results are summarized in Table II and compared with the theoretical predictions in

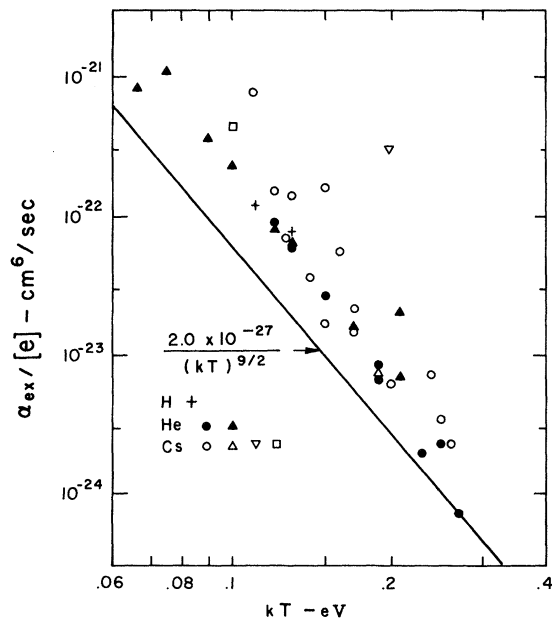


FIG. 12. Comparison of measured overall recombination-rate constant,  $a_{\text{ex}}$ , with theoretical calculation for excitation and de-excitation of atoms by electron impacts. The experimental results are coded as follows: + Hinnov and Hirschberg<sup>13</sup>;  $\blacktriangle$  Mohler and Kuckes,<sup>14</sup>  $\circ$  Aleskovskii,<sup>15</sup>  $\square$  Mohler,<sup>16</sup>  $\nabla$  D'Angelo and Rynn,<sup>17</sup> and  $\triangle$  Wada and Knechtli.<sup>18</sup>

TABLE II. Summary of experimental data and radiation correction factors. Column (1) gives the atom and code symbol, (2) the temperature, (3) the electron concentration, (4) Loschmidt number times the pressure in atmospheres, (5) the measured three-body recombination coefficient, (6) the energy in units of  $kT$  at which radiative and collisional de-excitation are equal, and (7) the radiation correction factor.

Atom	$kT$ (eV)	$10^{-13}[e]$ ( $\text{cm}^{-3}$ )	$10^{-13}[n]$ ( $\text{cm}^{-3}$ )	$10^{-23}\frac{a}{[e]}$ ( $\text{cm}^6 \text{sec}^{-1}$ )	$-\epsilon^*$	$a^*/a$	Ref.
H +	0.13	0.74	14	7.9	6.5	1.1	13
	0.11	0.47	7.0	11.8	6.8	1.1	
He ●	0.27	5.6	13.	0.072	5.6	1.3	13
	0.19	1.8	13.	0.72	5.6	1.3	
	0.13	0.62	13.	5.8	6.2	1.1	
	0.25	2.3	4.2	0.23	4.5	1.7	
	0.19	1.2	4.2	0.83	4.9	1.5	
	0.15	0.66	4.2	2.7	5.4	1.3	
	0.12	0.36	4.2	9.2	5.8	1.2	
	0.23	3.6	35	0.20	5.6	1.3	
He ▲	0.21	0.62	1.7	2.1	3.7	2.2	14
	0.12	0.31	1.7	8.7	5.6	1.3	
	0.09	0.15	1.7	37	6.2	1.1	
	0.075	0.065	1.7	108	5.8	1.2	
	0.21	1.8	14	0.72	4.5	1.7	
	0.17	1.2	14	1.6	5.6	1.3	
	0.13	0.61	14	6.1	6.2	1.1	
	0.10	0.31	14	23	6.7	1.1	
	0.066	0.16	14	88	8.5	1.0	
Cs ○	0.25	3.7	18	0.35	5.1	1.4	15
	0.20	3.1	18	0.63	6.1	1.2	
	0.17	1.6	18	2.2	6.1	1.2	
	0.16	0.75	18	5.6	5.3	1.3	
	0.15	0.40	18	16.3	4.7	1.6	
	0.24	2.7	53	0.74	4.9	1.5	
	0.17	1.7	53	1.5	6.2	1.1	
	0.14	0.89	53	3.6	6.3	1.1	
	0.13	0.55	53	6.2	6.0	1.2	
	0.26	5.9	350	0.23	5.6	1.3	
	0.15	1.7	350	1.7	7.0	1.1	
	0.13	0.40	350	14	5.5	1.3	
0.12	0.55	350	15	6.5	1.1		
0.11	0.14	350	79	5.0	1.4		
Cs □	0.1	0.08	100	44	4.6	1.6	16
Cs ▽	0.2	0.05	10	30	1.9	10	17
Cs △	0.19	0.40	10	0.75	3.7	2.2	18

Fig. 12. It can be seen that the data on H and He correlate remarkably well, but are slightly higher and exhibit a slightly steeper temperature dependence than the theory. The data on Cs scatter somewhat more, but exhibit the same general trend. This suggests that radiative cascading and collisions with neutrals may be contributing to the recombination rate.

To estimate the effect of radiation processes, we can compare the radiative and collisional de-

activation rates for a given atomic level. To calculate the radiative de-excitation rate, we use the expression<sup>19</sup>

$$A_n^r = (e^2/\hbar c)^3 (me^4/\hbar^3)n^{-4.5}, \quad (\text{IV. 19})$$

where  $n$  is the principal quantum number,  $c$  is the velocity of light, and  $\hbar$  is Planck's constant/ $2\pi$ . The collisional de-excitation rate obtained by

integrating Eq. (III.12) from  $-\delta$  to  $\epsilon_n$  is

$$A_n^e = \int_{-\delta}^{\epsilon_n} k(\epsilon, \epsilon_n) [e] d\epsilon$$

$$= 7.0 [e] \left( \frac{\hbar^3}{m^2 e^2} \right) \left( \frac{m e^4}{\hbar^2 k T} \right)^{0.17} n^{2.66}. \quad (\text{IV.20})$$

Thus, the ratio of collisional to radiative de-excitation is

$$\frac{A_n^e}{A_n^r} = 7.0 [e] \left( \frac{\hbar^3 c}{m e^4} \right)^3 \left( \frac{m e^4}{\hbar^2 k T} \right)^{0.17} n^{7.16}, \quad (\text{IV.21})$$

which shows that the relative importance of radiation increases extremely rapidly with decreasing  $n$ . The level  $n^*$  at which  $A_n^e/A_n^r = 1$  is given by

$$n^* = \left( \frac{2.1 \times 10^{17} [kT (\text{eV})]^{0.17}}{[e] (\text{cm}^{-3})} \right)^{0.14}, \quad (\text{IV.22})$$

and the corresponding energy in units of  $kT$  is

$$\epsilon^* = -1.9 \times 10^{-4} [kT (\text{eV})]^{-1.05} \times ([e] (\text{cm}^{-3}))^{0.28}. \quad (\text{IV.23})$$

For radiation to be negligible  $\epsilon^*$  must be several units below the "bottleneck" at  $-3.3$ . Reference to Table I shows that for most of the experiments under consideration  $\epsilon^*$  lies in the range  $-4$  to  $-8$ . Thus, while collisional de-excitation is the dominant process, radiation is not completely negligible. This conclusion is supported by the results in Fig. 11.

An approximate correction for radiative cascading can be made by assuming that the states below  $\epsilon^*$  are completely depopulated and imposing the boundary condition  $1 - \chi(\epsilon^*) = 0$  on the steady-state distribution function. This leads to the result

$$a^* \approx a \{3.3, \delta\}! / \{3.3, -\epsilon^*\}!, \quad (\text{IV.24})$$

which is compared to experiments in Fig. 13. It can be seen that the radiative correction reduces the scatter of the data somewhat, and improves the agreement between theory and experiment at high temperatures. The measured rates still exceed the theoretical prediction by a factor of 2 at low temperatures, however. Since the degree of ionization is relatively small in this region, a possible explanation is that collisional de-excitation by neutrals is contributing to the recombination rate. For this process to be significant, the cross section would have to be of the same

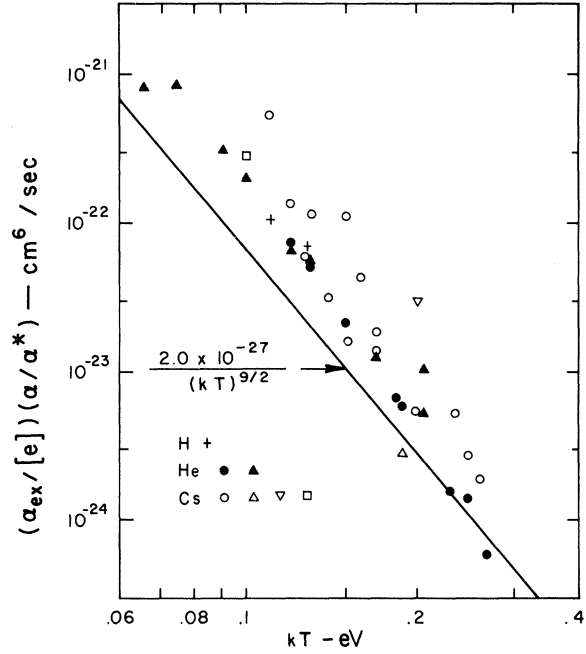


FIG. 13. Data of Fig. 12 approximately corrected for radiative cascading. The radiative correction reduces the scatter of the points somewhat, and improves the agreement with theory at high temperatures.

magnitude as the Coulomb cross section which seems rather unlikely. A more likely possibility is that dissociative recombination processes of the type



become important at low temperatures and low degrees of ionization.

A possible source of error in the theory is the assumption of a point core both in the variational integral and in the trajectory calculations. In reality the extended electron cloud and multiply-charged nucleus would give rise to a more complicated potential inside the cloud, even for an unperturbed core. Such an unperturbed potential would increase the rate integral  $\mathcal{R}_S$  by about 1% for helium or perhaps 10% for cesium. Moreover the incident electron will see a perturbed field, and may even exchange energy with the core electrons. Our trajectory calculations indicate that the two participating electrons are liable to pass inside the core during the course of the collision even though they are not likely to be there when they cross the surface  $E_1 = E_S$ ; that is, the core extension may affect  $f_S$  more than  $\mathcal{R}_S$ . It would be interesting to explore the effects of such an extended core on the trajectories. One might expect, however, that it has little influence on the distant, adiabatic collisions, whereas impulsive

collisions already have a high chance of succeeding, so that this chance would not be significantly increased.

In addition, the quantum-mechanical density of states is affected by the extended core, although this is predominant only for low-lying states below the bottleneck.

We conclude that for the experiments cited the recombination rate at high temperatures is controlled primarily by electron collisions and that the present theory gives a satisfactory account of this process. It is probable that radiation processes make a small contribution to the rate at high temperatures, and it is possible that dissociative recombination is important at low temperatures. Additional experiments at low temperatures and an analysis of the role played by dissociative recombination would be useful.

#### APPENDIX A

##### Approximate Evaluation of $\chi(\epsilon)$

To obtain  $\chi(\epsilon)$  from the transition kernel Eq.

(III. 6), we must evaluate integrals of the type

$$H(x) = \int_0^x f(y) y^p e^{-y} dy, \quad (\text{A. 1})$$

$$\text{where } f(y) = A(p+1+y)/(p+y)^2 \quad (\text{A. 2})$$

is a relatively slowly varying function of  $y$ . Although this integral cannot be done exactly, an excellent result can be obtained by approximating  $f(y)$  in the form

$$f(y) \approx f(p)(y/p)^a, \quad (\text{A. 3})$$

$$\text{where } a = d \ln f / d \ln y = (p+1)/(2p+1). \quad (\text{A. 4})$$

Substitution of Eq. (A. 3) into Eq. (A. 1) then gives

$$H(x) \approx [A(2p+1)/4p^{2+a}] \{p+a, x\}!, \quad (\text{A. 5})$$

where  $\{p, x\}!$  is the incomplete factorial defined by Eq. (IV. 17).

\*This research was supported by the Advanced Research Projects Agency of the Department of Defense and Space and Missile Systems Organization, Air Force Systems Command, and was monitored by Space and Missile Systems Organization, Air Force Systems Command under Contract No. F04701-68-C-0036.

†Present address: Physics Department, Brandeis University, Waltham, Mass.

‡Present address: Mechanical Engineering Department, Massachusetts Institute of Technology, Cambridge, Mass.

<sup>1</sup>J. C. Keck, *Discussions Faraday Soc.* **33**, 173 (1962).

<sup>2</sup>J. C. Keck, *J. Chem. Phys.* **32**, 1035 (1960); *Advan. Chem. Phys.* **13**, 85 (1967).

<sup>3</sup>B. Widom, *Advan. Chem. Phys.* **5**, 353 (1963).

<sup>4</sup>J. Keck and G. Carrier, *J. Chem. Phys.*, **43**, 2284 (1965).

<sup>5</sup>M. Gryzinski, *Phys. Rev.* **115**, 374 (1959).

<sup>6</sup>M. Gryzinski, *Phys. Rev.* **138**, A322 (1965).

<sup>7</sup>D. R. Bates, A. E. Kingston, and R. W. P. McWhirter, *Proc. Roy. Soc. (London)* **A267**, 297 (1962).

<sup>8</sup>A. V. Gurevich and L. P. Pitaevskii, *Zh. Eksperim. i Teor. Fiz.* **46**, 1281 (1964) [English transl.: *Soviet Phys. - JETP* **19**, 870 (1964)].

<sup>9</sup>R. Abrines, I. C. Percival, and N. A. Valentine, *Proc. Phys. Soc. (London)* **89**, 515 (1966).

<sup>10</sup>F. T. Wall, L. A. Hiller, and J. Mazur, *J. Chem. Phys.* **35**, 1284 (1961).

<sup>11</sup>B. Makin and J. Keck, *Phys. Rev. Letters* **11**, 281 (1963).

<sup>12</sup>The integration should be interpreted as a sum for discrete states.

<sup>13</sup>E. Hinnov and J. G. Hirschberg, *Phys. Rev.* **125**, 795 (1962).

<sup>14</sup>R. W. Motley and A. F. Kuckes, *Proceedings of the Fifth International Conference in Ionic Phenomena, Munich, 1961* (North-Holland Publishing Co., Amsterdam, 1961).

<sup>15</sup>Yu. M. Aleskovskii, *Zh. Eksperim. i Teor. Fiz.* **44**, 840 (1963) [English transl.: *Soviet Phys. - JETP* **17**, 570 (1963)].

<sup>16</sup>F. L. Mohler, *J. Res. Natl. Bur. Std. (U.S.)* **19**, 447 (1937).

<sup>17</sup>N. D'Angelo and N. Rynn, *Phys. Fluids* **4**, 1303 (1961).

<sup>18</sup>J. Y. Wada and R. C. Knechtli, *Proc. IRE* **49**, 1926 (1961).

<sup>19</sup>H. A. Bethe and E. E. Salpeter, *Quantum Mechanism of One- and Two-Electron Atoms*, (Academic Press, Inc., New York, 1957).